STM JOURNALS

Journal of
Polymer & Composites

ISSN: 2321-2810 (Online)
ISSN: 2321-8525 (Print)
Volume 13, Special Issue 3, 2025
DOI (Journal): 10.37591/JoPC

https://journals.stmjournals.com/jopc

Research JoPC

Wettability and Physiothermal Analysis of Silver-Reinforced Eggshell-Derived Hydroxyapatite Based Biocomposite

Gagan Bansal[1,*], Rakesh Kumar Gautam[2], Joy Prakash Misra[3], Chandra Kishore[4], Vartika Agarwal[5]

Abstract

Hydroxyapatite (HAp), a biocompatible ceramic material, has garnered significant interest in medical applications due to its natural bone type replica. The current study investigates the physical, wettability, and thermal properties of a novel HAp derived from eggshell waste and reinforced with silver nanoparticles at 0.0, 0.1, 0.2 and 0.5 weight % concentration using chemical precipitation method and termed as HAP0.0Ag, HAP0.1Ag, HAP0.2Ag and HAP0.5Ag respectively. As observed, the Fourier transform infrared spectroscopy (FTIR) and scanning electron microscopy (SEM) morphology confirms the synthesis of eggshell-derived silver-reinforced HAp, and doping improves the voids content in the material. The increase in contact angle from $66.20^0 \pm 2.80^0$ (HAP0.0Ag) to $71.35^0 \pm 1.45^0$ (HAP0.5Ag), decrease in calculated total SFE from 43.15 ± 0.32 (HAP0.0Ag) to 38.21 ± 0.36 (HAP0.5Ag) and decrease in water absorption by 21.31 % between unreinforced and 0.5% reinforced HAp reveals the surface hydrophobicity leading to improved wettability characteristics. The thermal stability and decomposition properties of the materials are assessed using Thermogravimetric analysis (TGA) and Derivative Thermogravimetric curve (DTG), and the results show 7- 8 % decomposition of HAp material when heated till 1000^0C, providing insights into their suitability for high- temperature applications. The overall analysis opens avenues for diverse use of silver-reinforced HAp, from implant coating to dental implants and catalytic supports.

Keywords: Hybrid composite, synthesis, hydroxyapatite, nanoparticles, biocomposites, biomedical applications

***Author for Correspondence**
Gagan Bansal

[1]Assistant Professor, Department of Mechanical Engineering, Graphic Era (Deemed to be University), Dehradun, Uttarakhand, India
[2]Professor, Department of Mechanical Engineering, Indian Institute of Technology (BHU) Varanasi, Uttar Pradesh, India
[3] Assistant Professor, Department of Mechanical Engineering, Indian Institute of Technology (BHU) Varanasi, Uttar Pradesh, India
[4]Associate Professor, Department of Mechanical Engineering, Graphic Era (Deemed to be University), Dehradun, Uttarakhand, India
[5]Assistant Professor, Department of Computer Applications, Graphic Era (Deemed to be University), Dehradun, Uttarakhand, India

Received Date: November 12, 2024
Accepted Date: December 17, 2024
Published Date: April 24, 2025

Citation: Gagan Bansal, Rakesh Kumar Gautam, Joy Prakash Misra, Chandra Kishore, Vartika Agarwal. Wettability and Physiothermal Analysis of Silver-Reinforced Eggshell-Derived Hydroxyapatite Based Biocomposite. Journal of Polymer & Composites. 2025; 13(Special Issue 3): S300–S314p.

INTRODUCTION

Biomaterials and biowaste utilization are the keys to sustainable development in the current research scenario [1]. Hydroxyapatite ($Ca_{10}(PO_4)_6(OH)_2$, HAp), a component of bone and teeth, has drawn much interest because of its potential for use in both medicinal and industrial applications [2,3]. In recent years, HAp has been synthesized from biowaste using a wide variety of synthetic processes, including hydrothermal [4], sol-gel, precipitation [5–7], Mechano-chemical [8], and mechanical activation methods. The high cost of the precursors, the complexity of the processes, the severe particle aggregation, and the low yield are just some of the issues that plague these methods. Chemical precipitation is the most promising method for producing HAp because it requires little energy, produces high yields and purity, results in homogenous mixing, and allows for precise control

over microstructure, porous size, Nanophase particle size, and the scale at which HAp is produced, among other benefits [9–12].

Biomedical uses for hydroxyapatite include soft tissue regeneration, scaffolds, bioactive coatings, bone fillers, and drug delivery systems. It has good biocompatibility and osteoconductive qualities, and its chemical make-up is comparable to that of the inorganic portion of human bone. Pure HAp has a stoichiometric ratio (Ca/P) of 1.67, resulting in the highest level of chemical stability. In most cases, porous scaffolds are used to implant HAp bioceramics. However, due to its compromised mechanical qualities, HAp has limitations in load-bearing applications [13]. In order to obtain hydroxyapatite with organic matter, plentiful eggshell debris can be employed as a source of calcium. The superior dissolution, biomineralization, and Osteointegration properties of eggshells make it an ideal starting material for synthesizing hydroxyapatite [14–17]. Chicken eggshell is used as the primary ingredient in this study because the calcination of the chicken eggshell has comparatively higher calcium oxide (CaO) purity than duck and quail eggshell [18,19].

The wettability of a material is a key factor in how it reacts with liquids, which affects everything from surface layers to medical implants. By looking at how wet this mixture is, its interaction with fluids has to be analyzed. Percentage of water absorption (WA%), contact angle (CA) measurement and total surface free energy (SFE) is used to identify the wettability behavior of the material. Similarly, thermal analysis is necessary to comprehend the response to temperature and stress changes for any material. The TGA and DTG investigation must be evaluated to identify the decomposition rate during high-temperature applications. The research results may help pave the way for creating high-end biomaterials with tailored qualities, fostering creativity, facilitating technological progress, and improving people's health in numerous ways [20].

A large number of research publications are available on the synthesis and characterization of HAp and metal-reinforced HAp [21]. Also, the works of literature are available on various synthesis methods and resources for extracting HAp [22–25]. Unfortunately, the effective wettability and physiothermal characterization of eggshell-derived silver-reinforced HAp is not currently available. However, Maidaniuc et al. [26] examined the induced wettability and surface volume correlation of Bovine bone-derived HAp for enhanced oil recovery applications. Mirzaee et al. [27] synthesized HAp using the sol-gel technique and reported the antibacterial nature of silver-reinforced HAp. Similarly, several authors [28–32] experimentally determined the antibacterial characteristics of silver doping in commercially available HAp. Recently, Vijayaraghavan et al. [33] synthesized silver-reinforced HAp but used eggshell bone of black Sumatra as a calcium precursor and reported antibacterial nature in gram-positive and gram-negative microorganisms. Nurfiana et al. [34] used duck eggshells and synthesized silver-reinforced HAp for antibacterial applications. Therefore, the literature confirms the antibacterial nature of silver-reinforced HAp. The current research was performed for the thermal and wettability analysis of the silver-reinforced eggshell-derived HAp. Fig 1. highlights the brief objective of the current research.

In the present investigation, the eco-friendly and biocompatible silver-reinforced hydroxyapatite was synthesized using waste eggshell through modified synthesis route i.e., multistage calcination followed by a chemical precipitation method. The novel combination of heat and water was used for the characterization. The study aimed to analyze the wettability and the Physiothermal behavior of a bioceramic material synthesized using a varying molar concentration of silver doping in HAp. The FTIR and SEM characterizations were performed to examine the formation of functional groups and morphology of the synthesized powdered samples. The wettability behavior on the sintered samples was diagnosed by measuring the contact angle, total surface free energy and water absorption percentage. However, the thermal analysis was done by determining the TGA and DTG curves of the samples to examine their decomposition and phase transformation temperatures. The experimental density, relative density, porosity and morphology were determined to study the physical nature of the eggshell-derived silver-reinforced HAp. Collectively, these characterizations expose an eco-friendly and novel biomaterial with high thermal stability and acceptable wettability characteristics.

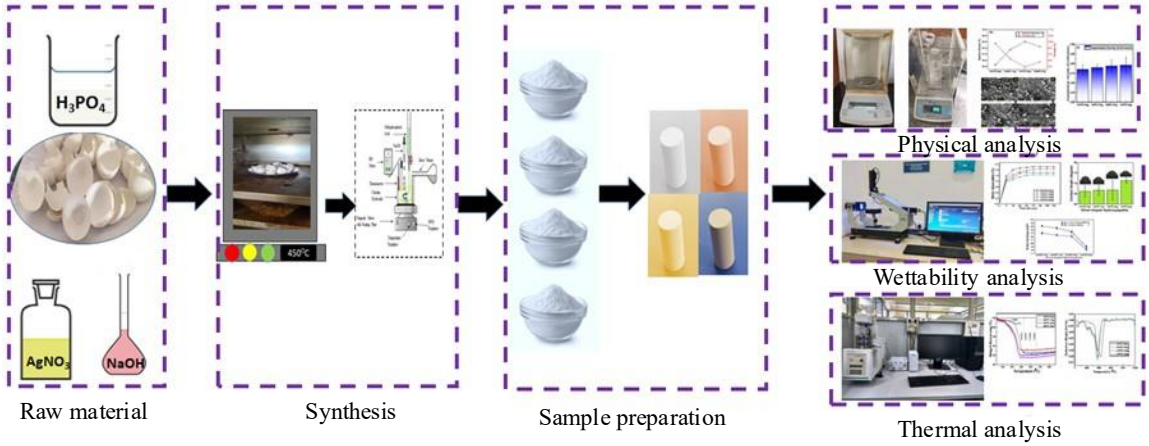

Figure 1. Schematic diagram of the synthesis and characterization of silver-reinforced Hap.

MATERIALS AND METHODS

Materials

Waste eggshells collected from Hostel mess (GEU, Dehradun), Orthophosphoric acid (H_3PO_4) (extra pure, 1.70g/mL (at 20^0C)), silver nitrate ($AgNO_3$) (assay 99.8 %) purchased from SRL Pvt. Ltd, Mumbai, India and NaOH (assay 97 %) purchased from AMIL, Thane, India.

Synthesis of Eggshell-Derived Silver-Reinforced Hydroxyapatite

The waste chicken eggshells collected from the hostel's mess (GEU Dehradun) were washed and boiled in distilled water at 110^0C for 30 min to remove all undesired contaminations and semipermeable inner shell membranes. After that, the eggshells were dried in an electric oven for 3 hours at 120^0C and then crushed using a mortar and pestle. The cleaned eggshells were subjected to multistage calcination at 200 °C, 450 °C, 650 °C, 900 °C, and 1050 °C with a dwell period of 10 minutes and thorough mixing. The $Ca(OH)_2$ formed using eggshell waste acts as a calcium precursor, and Orthophosphoric acid as a phosphorous precursor. The synthesis parameters are mentioned in Table 1. The calculated amount of precursors was added and synthesized using the chemical precipitation method, with slow addition of defined molar concentrated $AgNO_3$ (0.2mL/min) for doping and vigorous stirring for 18 h at 660 rpm and 55 ^{0}C. Later the precipitate was separated from the suspension by decanting 5- 7 times. Finally, the precipitate was dried in an electric oven at 120 ^{0}C for 24 hours and kept for another 24 h inside a closed oven. Four combinations formed by doping 0, 0.1, 0.2 and 0.5 molar % concentration of $AgNO_3$ in HAp were nomenclate as HAP0.0Ag, HAP0.1Ag, HAP0.2Ag and HAP0.5Ag.

Pellet Sample Preparation

The synthesized HAPAg powder was firstly ball milled using high-energy planetary ball milling (RETSCH PM400) for size uniformity. The pallets of 10 mm dia are prepared through die steel compression die using uniaxial pressure of 318 MPa for 60 sec. The compacted samples are further sintered in a muffle furnace at 900 ^{0}C for 1 h at 5 ^{0}C/min ramp rate and 2 h socking time. The prepared samples were preserved in the vacuum desiccator till it was used for investigation and characterization.

Table 1. Parameters used in the Synthesis of Eggshell-Derived Silver-Reinforced HAp

Parameters	Values
Precursor (calcium)	Waste Eggshells
Precursor (phosphorous)	H_3PO_4 (extra pure)
Calcination Temperature	1050 ^{0}C (maximum)
Initial molar concentration (Ca/P)	M
Synthesis time	18 h
Temperature	55 ^{0}C
Stirring Speed	660 rpm
Ag doping molar percentage	0.1, 0.2 and 0.5

CHARACTERIZATIONS

Wettability Analysis

The water absorption test, contact angle measurement and surface free energy analysis were amalgamated to analyze the wettability characteristics of silver-reinforced HAp samples.

Water Absorption Test

The ASTM D 570-98 standard was followed for the water absorption test. The absorbed water content of the composite samples was determined after immersing the sample in distilled water at room temperature for the prescribed duration. The accurate weight of the sample was measured using an electronic weighing machine (Model AR2140, Essae Teraoka Ltd.) with an accuracy of 0.0001 g. The dry weights (W_{dry}) of the composite samples were measured prior to immersion, and their wet weights (W_{wet}) were measured after immersion in water for 8 h, 16 h, 24 h, 48 h, 72 h, 96 h, 120 h and 144 h. The weight measurement was taken at least three times per observation per sample. The water absorption % (W_a (%)) was determined using equation (i).

$$W_a\ (\%) = (W_{wet} - W_{dry})/\ W_{dry} \times 100\ \% \ . \quad \text{(i)}$$

Contact Angle Measurement

The Contact angle measurement machine (model: DSA 25S, Kruss Germany) measures the hydrophobicity/ hydrophilicity of the composite sample using sessile drop orientation of water/ethanol droplet with tangent fitting and manual baseline correction. The contact angle above and below 90^0 represents the degree of hydrophobicity and hydrophilicity, respectively, of the composite samples. The average of minimum of 5 drops is considered for determining the contact angle for wettability analysis.

Surface Free Energy

The direct magnitude of surface free energy (SFE) is obtained through a contact angle measurement machine (model: DSA 25S, Kruss Germany) using the contact angle (θ) of deionized water and diazomethane droplets. Also, the values of contact angle obtained are used for evaluating the surface free energy (SFE) of a material (E_s) using equations (ii and iii) termed as Owens Wendt Equation [35]. The equation helps to determine the polar and dispersive components of SFE, which further determines the total SFE at any particulate contact angle.

$$\frac{1+\mathrm{Cos}\theta}{2} = \sqrt{\mathrm{E_S^d}}\left(\frac{\sqrt{\mathrm{E_l^d}}}{\mathrm{E_l}}\right) + \sqrt{\mathrm{E_S^p}}\left(\frac{\sqrt{\mathrm{E_l^p}}}{\mathrm{E_l}}\right) \quad \text{(ii)}$$

$$\mathrm{E_s} = \mathrm{E_S^d} + \mathrm{E_S^p} \quad \text{(iii)}$$

Where,

$\mathrm{E_l} =$ surface free energy of liquid droplet (diiodomethane $= \frac{50.8\mathrm{mJ}}{\mathrm{m^2}}$ and water $= \frac{72.8\mathrm{mJ}}{\mathrm{m^2}}$)

$\mathrm{E_S^d} =$ Dispersive component of SFE

$\mathrm{E_S^p} =$ Polar component of SFE

$\mathrm{E_l^d} =$ Dispersive component of liquid $\left(\text{diiodomethane} = \frac{50.8\mathrm{mJ}}{\mathrm{m^2}} \text{ and water} = \frac{20.8\mathrm{mJ}}{\mathrm{m^2}}\right)$

$\mathrm{E_l^p} =$ Polar component of liquid (diiodomethane $= 0$ and water $= \frac{51\mathrm{mJ}}{\mathrm{m^2}}$)

Thermal Analysis

It is possible to recognize and describe the different types of thermal events occurring in a sample by analyzing the DTG curve along with the TG curve and other thermal analysis data. This knowledge is helpful in disciplines like materials science, chemistry, and process engineering, where a grasp of thermal behavior is essential for quality assurance, research, and development.

Thermogravimetric Analysis (TGA)

The TGA was performed to analyze the degradation of material with temperature using TGA-50, 220/240V machine manufactured by M/s Shimadzu (Asia Pacific Pvt. Ltd.). The temperature range was taken from room temperature to 1000^0C, ramping rate of 10^0C/min under a nitrogen-based inert atmosphere with a maximum 10mg sample weight placed in a platinum crucible.

Derivative Thermogravimetric Analysis (DTG)

The DTG curve (derivative weight (%/min) v/s temperature (^{0}C)) refers to the first derivative of the smooth Thermogravimetric (TG) curve that represents the sample's weight change during cooling or heating. The peaks on the DTG curve represent the area where the highest rate of weight change is observed, i.e., the temperature at which rapid decomposition or volatilization of the component occurs. Valleys indicate the stable region where minimal change is observed mainly due to steady-state conditions or phase translation.

Experimental Density and Porosity Percentage Calculation

The experimental density of the sintered samples was determined using Archimedes' principle by accurately measuring its suspended weights in air and distilled water ($\rho = 1 g/cm^3$). The Wensar HPB220 (220 g capacity; 0.0001g readability) density measuring equipment was used to calculate density. The average and standard deviation of a minimum of three readings were considered for determining the final magnitude of each sample. The weight fraction method determined the theoretical density, and the relative density and porosity percentages were further calculated using the obtained values.

Morphological Characterization

Fourier Transform Infrared Spectroscopy (FTIR): The FTIR spectroscope (Model: Nicolet iS5 by Thermo Electron Scientific Instruments LLC) identifies functional groups and bonding characteristics using KBr Technique. Operating parameters include two spectrums with a $LiTaO_3$ detector, 5 ^{0}C- 45 ^{0}C temperature range and eight split frequency range 4250- 250cm^1.

Scanning Electron Microscopy

The SEM. (EVO – SEM MA15/ 18 model, manufactured by Carl Zeiss Microscopy Ltd.) was used for morphological characterization under 39 ^{0}C ambient temperature with 52 % RH. The SEM micrographs at 500X magnification are taken in the current analysis.

RESULT AND DISCUSSIONS

Figure 2 shows the FTIR curves of the silver-reinforced hydroxyapatite powder, and the interpretations of the peaks and valleys at various wave numbers are tabulated in Table 2. Fingerprint region (450-1500 cm^{-1}) contains the maximum peaks. The perceptibility of O-P-O bending mode near 607.23 cm^{-1} and 657.01cm^1 [36], parallel P-O bond between 1050 cm^{-1}- 850 cm^{-1} [37], asymmetric stretching bond of O-P-O at 1065.84 cm^{-1}, 987.55 cm^{-1} and 861.61 cm^{-1} [38,39], v_2 stretching bond of OH functional group at 1631.09 cm^{-1} and 3329.47 cm^{-1} and silver-based bonding at 1065 - 1100 cm^{-1} [40] reveals the presence of desired functional groups in the synthesized HAp powder.

Figure 3 highlights the SEM morphology of HAP0.0Ag, HAP0.1Ag, HAP0.2Ag and HAP0.5Ag powder at 500 X magnification. The morphology indicates the uniformity in the shape and size of the synthesized samples. Also, the non-visibility of any individual dispersion of silver particles indicates that the Ag ions are well accommodated in the crystal structure of HAp through chemical synthesis. However, a small reduction in the average particle size with the increase in doping concentration was observed in the analysis.

The experimental, theoretical and relative density of the prepared HAPAg pellet samples were determined with a high level of accuracy. Figure 4(a) shows the calculated experimental density of the eggshell-derived silver-reinforced HAp pellet samples. The experimental density of HAP0.0Ag, HAP0.1Ag, HAP0.2Ag and HAP0.5Ag. are 2.84 ± 0.12, 2.90 ± 0.08, 2.93 ± 0.16 and 2.96 ± 0.20 g/cm^3

respectively. The increase in the density with an upsurge in silver doping was observed. The calculated theoretical density of HAP0.0Ag, HAP0.1Ag, HAP0.2Ag and HAP0.5Ag. are 3.16, 3.174, 3.189 and 3.23 g/cm^3. Also, the relative density (shown in Fig 4(b)) of HAP0.0Ag, HAP0.1Ag, HAP0.2Ag and HAP0.5Ag. are 90.12 %, 91.37 %, 92.03% and 91.62 % respectively. The maximum relative density of HAP0.2Ag composition shows the minimum porosity percentage (7.97 %) and high compactness. The sample's relative density helps to determine the strength and hardness [14] of the sintered material.

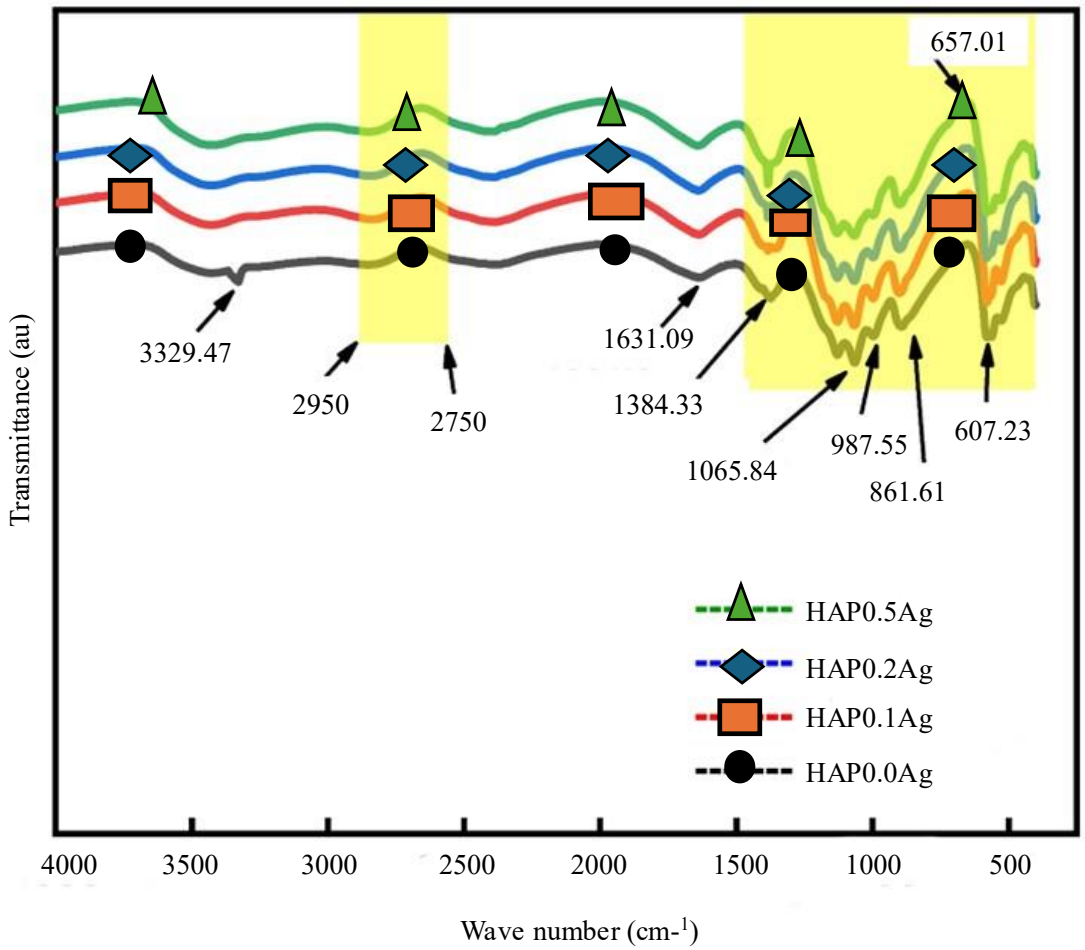

Figure 2. FTIR spectra of silver-reinforced eggshell-derived hydroxyapatite.

Table 2. FTIR interpretations at different wave numbers.

Wave number	Interpretation	Reference
607.23 cm^{-1}	O-P-O bending mode	Sebastiammal et al. [36].
657.01 cm^{-1}	O-P-O bending mode	Sebastiammal et al. [36].
1050 cm^{-1}- 850 cm^{-1}	$PO4^{3-}$ functional group and parallel P-O vibrations	Ganesan et al. [37]
1065.84 cm^{-1}, 987.55 cm^{-1} and 861.61 cm^{-1}	large intensity v_3 asymmetric stretching mode of O-P-O	Kumar et al. [38] and Chappard et al. [39]
1631.09 cm^{-1} and 3329.47 cm^{-1}	v_2 bending mode of the O-H functional group	Chappard et al. [39]
1384.33cm^{-1}	silver-based bonding	Iconaru et al. [40]
1065 - 1100 cm^{-1}	due to silver doping	Iconaru et al. [40]
Broadband 2750cm^{-1} - 2950cm^{-1}	symmetric stretching of hydrated silver-reinforced HAp	Kumar et al. [38],

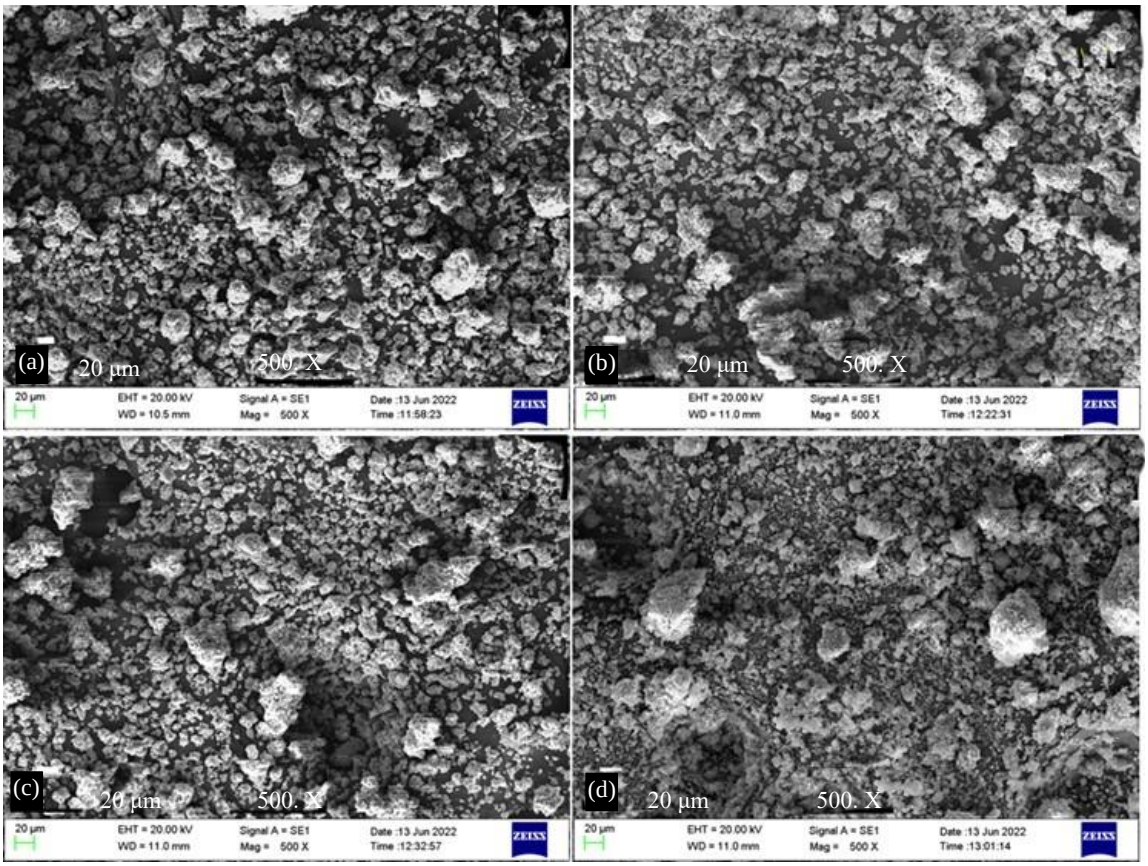

Figure 3. SEM morphology of (a) HAP0.0Ag, (b) HAP0.1Ag, (c) HAP0.2Ag and (d) HAP0.5Ag powder at 500 X magnification.

Water absorption tests on the synthesized samples were performed for six days. The percentage of water absorbed with time is plotted as shown in Fig 5. The initial dried sample of HAP0.0Ag, HAP0.1Ag, HAP0.2Ag and HAP0.5Ag weighed 1.56 g, 1.82 g, 1.61 g and 2.11 g, respectively, and it was increased by 1.49 %, 1.32 %, 1.25 % and 1.16 % after eight h of immersion. The sample weights were taken continuously until the constant mass between three consecutive readings was observed. The maximum water absorption was observed in unreinforced HAp (HAP0.0Ag, 1.974 %) after 144 h. As observed, the Ag doping improves the water-socking ability of the samples, and thus the reduction in open pores is interpreted. The percentage of water absorption also decreases with an increase in Ag doping concentration in HAp and divulges the slight hydrophobicity of reinforced samples, which is also testified during contact angle measurement. Reis et al. reported increased flexural strength of an acrylic-based denture resin after 30 days of immersion [41]. The flexural change could be due to the continuous polymerization of the monomer, which acts as a plasticizer and leaches from the specimen to increase flexural strength. The specimen's weight variation was a combination of weight rise due to absorption and weight loss caused by sample leaching [42].

The wettability of the silver-reinforced hydroxyapatite samples examined using contact angle is shown in Figure 6. The average ± SD value of the contact angle for HAP0.0Ag, HAP0.1Ag, HAP0.2Ag and HAP0.5Ag are 66.2 ± 2.8, 66.75 ± 2.45, 66.85 ± 4.85 and 71.35 ± 1.45 respectively. The values thus obtained show the hydrophilic nature of the HAPAg samples. The low contact angle for HAp promotes higher surface courage in coating applications [43]. The hydrophilic material exhibits better results in biomedical applications, diagnostic devices, drug delivery, surface coating, heat dissipation and hydrogel applications. Maidaniuc et al. [26] reported that the contact angle of HAp was influenced by particle size and forming pressure.

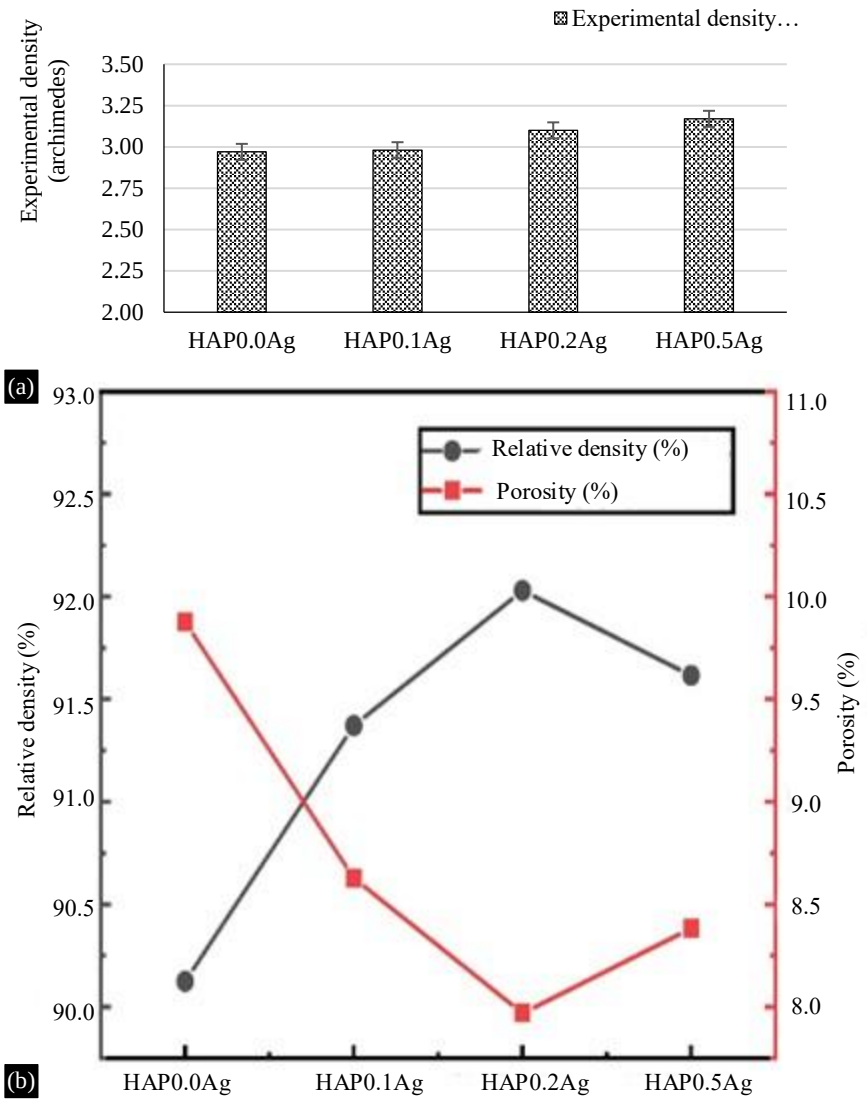

Figure 4. (a) Experimental density, and (b) Relative density and porosity of silver-reinforced hydroxyapatite.

The calculated and the direct magnitude of SFE for the silver-reinforced hydroxyapatite samples are graphed in Figure 7.SFE contributes to cell adhesion to HAp through wettability [44]. It is the inverse of the contact angle and influences an implant's biological interactions [45]. The calculated values are obtained using Owens Wendt Equation [35], while the direct values were obtained from the contact angle measurement machine (model: DSA 25S, Kruss Germany) through distilled water and diazomethane droplets. The decrease in the mean values of total SFE with the increase in doping concentration reveals the hydrophobicity of the silver-reinforced samples, which directly correlates with the water absorption % and the contact angle. The E_s^d and E_s^p values for HAP0.0Ag was 29.43 mJ/m^2 and 13.62 mJ/m^{2,} whereas HAP0.5Ag decreased to 26.28 mJ/m^2 and 11.92 mJ/m^2, respectively. The mean ± SD of the contact angle and SFE are tabulated in Table 3. SFE determines the wettability and adhesion characteristics of the liquid with solid surfaces [44]. Szcześ et al. [46] compared the SFE between synthetic and natural (obtained from pig bones) HAp using the thin-layer wicking method and concluded that the average total SFE for natural HAp is slightly higher than synthetic HAp. However, the result obtained in the current research has a total SFE lower than that reported by Szcześ et al. [46]. The variation in the precursor, the methodology adopted, and doping concentration directly affect total SFE magnitude.

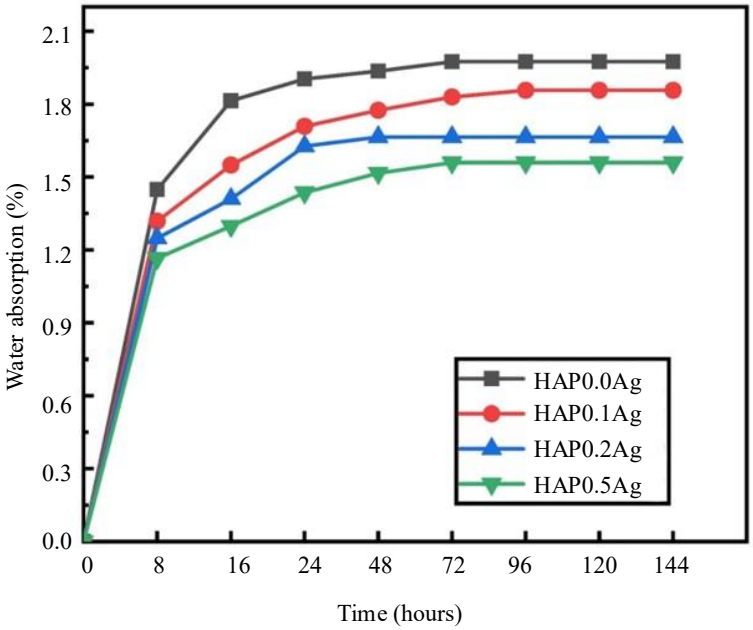

Figure 5. Water absorption (%) of silver-reinforced hydroxyapatite composite with time (hours).

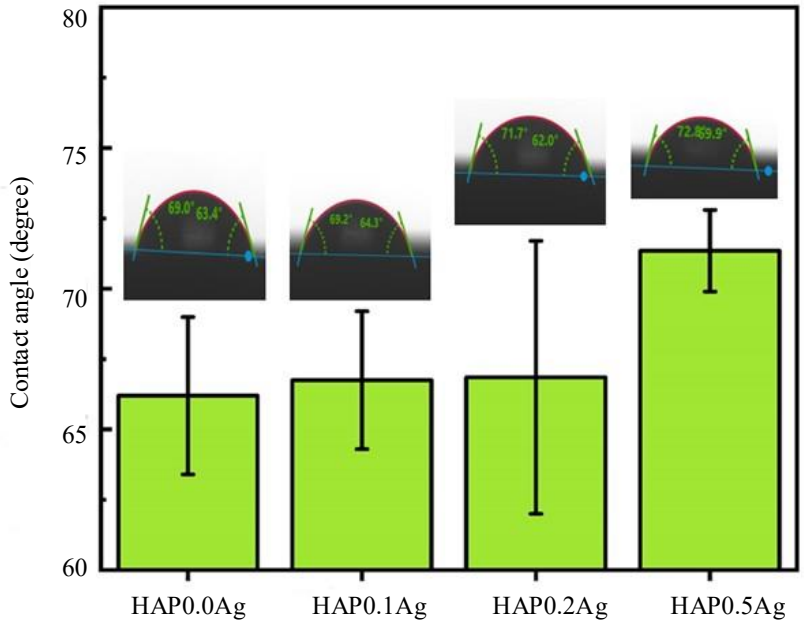

Figure 6. Contact angle of silver reinforced hydroxyapatite.

TGA results of the powdered samples are illustrated in Figure 8 (a). The curve represents the percentage of weight loss with the increased temperature of the synthesized powder. As observed, the mass decomposition was between 6.9- 8.4% till 1000^0C, depending upon the doping concentration of the powdered sample. The initial weight loss between 23-250^0C is attributed to the absorbed water during chemical synthesis [47]. The degradation in the mass near 250^0C- 450^0- corresponds to the conversion of hydrogen phosphate to phosphate via pyrophosphate, releasing water of hydration as shown in equations (iv and v).

$$2HPO_4^{2-} \rightarrow P_2O_7^{4-} + H_2O \uparrow \quad \text{(iv)}$$

$$P_2O_7^{4-} + 2OH^- \rightarrow 2PO_4^{3-} + H_2O \uparrow \quad \text{(v)}$$

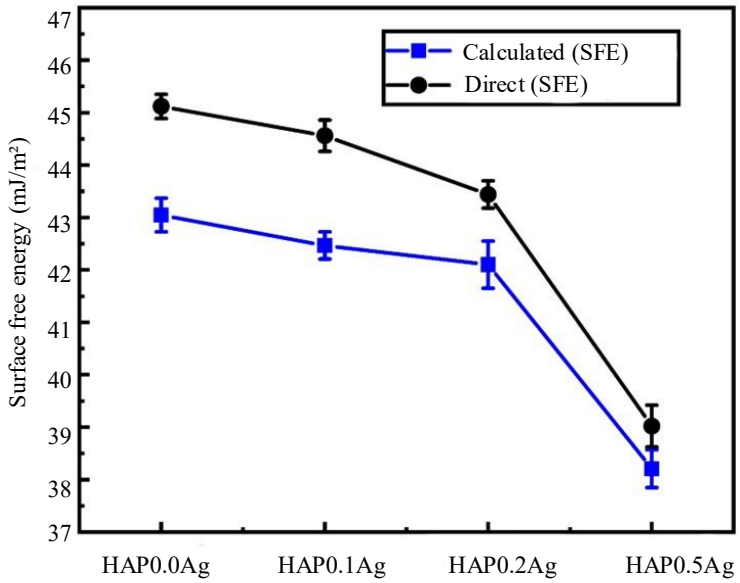

Figure 7. Surface free energy of the silver-reinforced hydroxyapatite

Table 3. Contact angle and surface free energy values for silver-reinforced hydroxyapatite samples.

Sample	Contact angle		Total surface free energy		% Error
	water droplet	*Diiodomethane droplet*	*Calculated*	*Instrumental*	
HAP0.0Ag	66.20 ± 2.80	58.40 ± 1.41	43.05 ± 0.32	45.12 ± 0.23	4.81
HAP0.1Ag	66.75 ± 2.45	59.17 ± 1.82	42.47 ± 0.26	44.56 ± 0.30	4.92
HAP0.2Ag	66.85 ± 4.85	60.12 ± 3.12	42.10 ± 0.45	43.44 ± 0.26	3.18
HAP0.5Ag	71.35 ± 1.45	63.89 ± 2.12	38.21 ± 0.36	39.02 ± 0.40	2.12

The minimum mass loss (6.935%) was observed in HAP0.1Ag and the maximum (8.388%) in HAP0.5Ag. The mass loss rate in HAP0.0Ag is minimum till 350^0C. However, the total mass loss in HAP0.0Ag was observed to be 7.4776% which is 0.54% more than the HAP0.1Ag, which can be due to the decomposition of the phosphate phase in unreinforced HAp or the interstitial water loss reported by Lazic et al. [48]. Also, silver doping may act as a binding agent when treated at higher temperatures. Mass loss in HAP0.2Ag retains 92.29% of the total mass till 1000^0C.

The degradation rate is minimal in unreinforced HAp and shows increasing trends with an increase in silver doping. HAP0.5Ag has a maximum mass loss, and the loss is at a comparatively lower temperature than other sequential compositions. It may be due to the release of nitrate ions, as nitrates are easily replaceable. It is interesting to note that the HAP0.0Ag and HAP0.1Ag curves cross at 456.23^0C. The remaining weight of sample HAP0.0Ag and HAP0.1Ag at an instant is the same, i.e., 93.155%. It is the instantaneous temperature where both compositions have the same degradation rate. It implies that the molar concentration of silver less than 0.1 can also be the optimum composition for thermally stable silver-reinforced HAp. A similar observation was seen in Figure 4 (b), where the porosity and relative density curve meets between zero and 0.1% doping. The DTG curve in Figure 8 (b) shows the deformation in phase near 400 ^{0}C where the weight derivative measured in weight remaining percent per min is minimum magnitude between 350-450 ^{0}C. The curve helps to determine the temperature associated with the phase transformation [49]. The rate of mass decomposition depends upon the percentage of doping in the HAp. It is probably because the increase in temperature first decomposes the impurity present in the stable calcium hydroxyapatite, which is highest in HAP0.5Ag. The negligible mass loss between 500 and 1000^0C concludes and confirms the high thermal stability of HAp at higher temperatures.

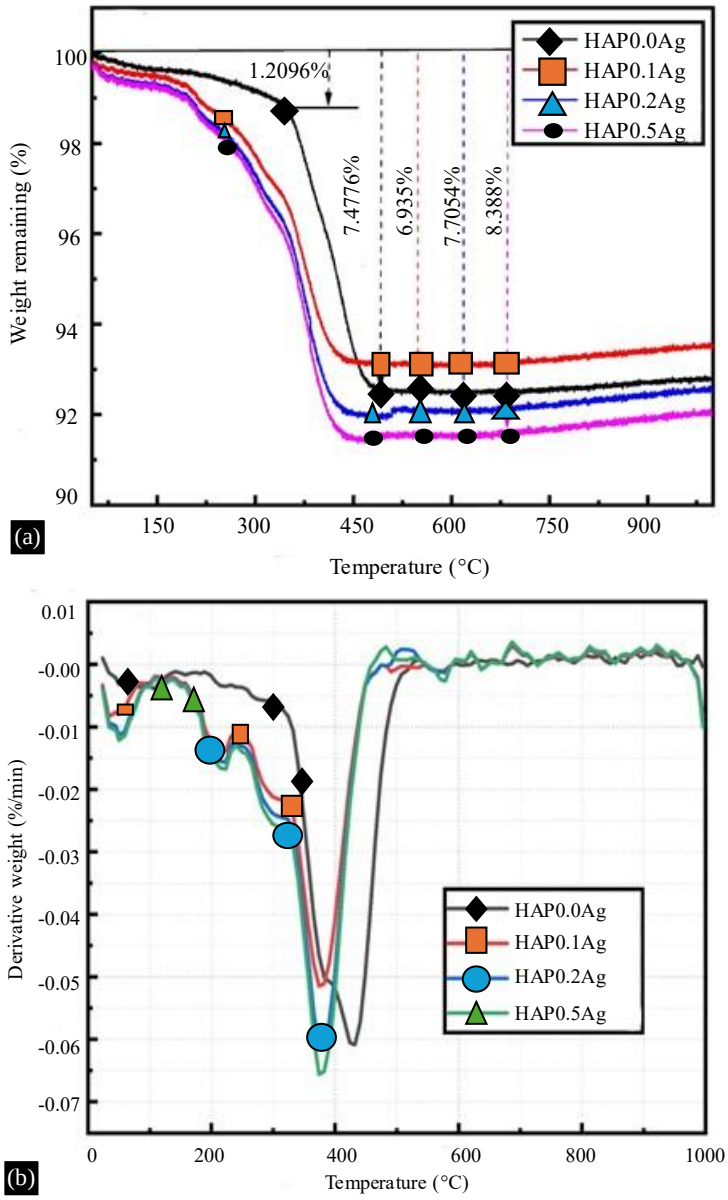

Figure 8. (a) Thermal gravimetric analysis (TGA) and (b) derivative thermogravimetric (DTG) Curve of eggshell-derived silver-reinforced Hap.

CONCLUSION

Eggshell-derived silver-reinforced HAp was synthesized using a modified chemical precipitation method and characterized in the current research. The physical analysis reports the increase in density with the increase in silver doping concentration in HAp and the minimum porosity (7.97 %) observed in the HAP0.2Ag sample. The wettability analysis concludes the hydrophilic nature of the prepared samples with a contact angle change from $66.2^0 \pm 2.8^0$ (HAP0.0Ag) to $71.35^0 \pm 1.45^0$ (HAP0.0Ag). The variation is predicted to be due to the decrease in SFE with the increase in doping percentage. Moreover, the minimum porosity and maximum relative density were observed in the HAP0.2Ag composition. The minimal upsurge in the material decomposition with silver doping at higher temperatures related to the decay of the Ag phase in the reinforced samples between 300-450 ^{0}C. However, the synthesized HAp possesses high thermal stability and can be useful for antibacterial and high-temperature coating applications. The obtained results conclude the high Physiothermal and wettability characteristics of the synthesized samples. Further, the synthesis and characterization parameters could be altered and explored as a future perspective on the current findings.

Acknowledgment

The authors thank the AICTE- QIP, India, Department of Mechanical Engineering, IIT (BHU) Varanasi, Graphic Era Deemed to be University, Dehradun and CIF, IIT (BHU) for providing all kinds of guidance and support in carrying out the current experimental research.

Declaration Of Conflicting Interests

The authors declare that there is no conflict of interest.

Funding

The authors received no financial support for this article's research, authorship, and/or publication.

REFERENCES

1. I. Abdulrahman, H.I. Tijani, B.A. Mohammed, H. Saidu, H. Yusuf, M. Ndejiko Jibrin, S. Mohammed, From Garbage to Biomaterials: An Overview on Egg Shell Based Hydroxyapatite, J. Mater. 2014 (2014) 1–6. https://doi.org/10.1155/2014/802467.
2. S. Balhuc, R. Campian, A. Labunet, M. Negucioiu, S. Buduru, A. Kui, Dental Applications of Systems Based on Hydroxyapatite Nanoparticles—An Evidence-Based Update, Crystals. 11 (2021) 674. https://doi.org/10.3390/cryst11060674.
3. S. Das Lala, P. Deb, E. Barua, A.B. Deoghare, S. Chatterjee, Characterization of hydroxyapatite derived from eggshells for medical implants, Mater. Today Proc. 15 (2019) 323–327. https://doi.org/10.1016/j.matpr.2019.05.012.
4. T.T. Hoai, N.K. Nga, L.T. Giang, T.Q. Huy, P.N.M. Tuan, B.T.T. Binh, Hydrothermal Synthesis of Hydroxyapatite Nanorods for Rapid Formation of Bone-Like Mineralization, J. Electron. Mater. 46 (2017) 5064–5072. https://doi.org/10.1007/S11664-017-5509-6.
5. M. Malakauskaite-Petruleviciene, Z. Stankeviciute, A. Beganskiene, A. Kareiva, Sol–gel synthesis of calcium hydroxyapatite thin films on quartz substrate using dip-coating and spin-coating techniques, J. Sol-Gel Sci. Technol. 71 (2014) 437–446. https://doi.org/10.1007/s10971-014-3394-5.
6. A.Ç. Kılınç, S. Köktaş, A.A. Göktaş, Characterization of eggshell-derived hydroxyapatite on Ti6Al4V metal substrate coated by sol–gel method, J. Aust. Ceram. Soc. 57 (2021) 47–53. https://doi.org/10.1007/s41779-020-00511-y.
7. A. Jaafar, C. Hecker, P. Árki, Y. Joseph, Sol-gel derived hydroxyapatite coatings for titanium implants: A review, Bioengineering. 7 (2020) 1–23. https://doi.org/10.3390/bioengineering7040127.
8. A. Pal, S. Maity, S. Chabri, S. Bera, A.R. Chowdhury, M. Das, A. Sinha, Mechanochemical synthesis of nanocrystalline hydroxyapatite from Mercenaria clam shells and phosphoric acid, Biomed. Phys. Eng. Express. 3 (2017) 015010. https://doi.org/10.1088/2057-1976/aa54f5.
9. C. Suresh Kumar, K. Dhanaraj, R.M. Vimalathithan, P. Ilaiyaraja, G. Suresh, Hydroxyapatite for bone related applications derived from sea shell waste by simpleprecipitation method, J. Asian Ceram. Soc. 8 (2020) 416–429. https://doi.org/10.1080/21870764.2020.1749373.
10. A. Yelten-Yilmaz, S. Yilmaz, Wet chemical precipitation synthesis of hydroxyapatite (HA) powders, Ceram. Int. 44 (2018) 9703–9710. https://doi.org/10.1016/j.ceramint.2018.02.201.
11. H. Peng, J. Wang, S. Lv, J. Wen, J.F. Chen, Synthesis and characterization of hydroxyapatite nanoparticles prepared by a high-gravity precipitation method, Ceram. Int. 41 (2015) 14340–14349. https://doi.org/10.1016/j.ceramint.2015.07.067.
12. D.G. Nelson, J.D. Featherstone, Preparation, analysis, and characterization of carbonated apatites., Calcif. Tissue Int. 34 Suppl 2 (1982) S69-81. http://www.ncbi.nlm.nih.gov/pubmed/6293677.
13. S. Panda, C.K. Biswas, S. Paul, A comprehensive review on the preparation and application of calcium hydroxyapatite: A special focus on atomic doping methods for bone tissue engineering, Ceram. Int. 47 (2021) 28122–28144. https://doi.org/10.1016/j.ceramint.2021.07.100.
14. S. Das Lala, E. Barua, P. Deb, A.B. Deoghare, Physico-chemical and biological behaviour of eggshell bio-waste derived nano-hydroxyapatite matured at different aging time, Mater. Today Commun. 27 (2021). https://doi.org/10.1016/j.mtcomm.2021.102443.

15. G. Bansal, R.K. Gautam, J.P. Misra, A. Mishra, Tribological behavior of silver-doped eggshell-derived hydroxyapatite reinforcement in PMMA-based composite, (2024). https://doi.org/10.1177/14644207241240623.
16. G. Bansal, R.K. Gautam, J.P. Misra, A. Mishra, Coating Methods for Hydroxyapatite—A Bioceramic Material, in: 2023: pp. 279–302. https://doi.org/10.1007/978-981-99-3549-9_13.
17. A.R.S. Manral, N. Gariya, G. Bansal, H.P. Singh, A. Rawat, Computational stress analysis of Chicken Feather Fibre (CFF) with Epoxy-Resin matrix composite material, in: Mater. Today Proc., 2019. https://doi.org/10.1016/j.matpr.2020.02.582.
18. G. Bansal, V.K. Singh, P.C. Gope, A. Jain, Thermal Characterization , Compositional Analysis and Extraction of Elemental Powder from Rohu Fish Residue used as Composite Particulate, 5 (2017) 25–33.
19. A. Mishra, P.K. Mishra, G. Bansal, Recent advances in coating characterization techniques, Dyn. Mech. Creep-Recovery Behav. Polym. Compos. (2024) 461–484. https://doi.org/10.1016/B978-0-443-19009-4.00024-2.
20. S. Santhosh, S. Balasivanandha Prabu, Thermal stability of nano hydroxyapatite synthesized from sea shells through wet chemical synthesis, Mater. Lett. 97 (2013) 121–124. https://doi.org/10.1016/j.matlet.2013.01.081.
21. A. Szcześ, L. Hołysz, E. Chibowski, Synthesis of hydroxyapatite for biomedical applications, Adv. Colloid Interface Sci. 249 (2017) 321–330. https://doi.org/10.1016/J.CIS.2017.04.007.
22. T. Varadavenkatesan, R. Vinayagam, S. Pai, B. Kathirvel, A. Pugazhendhi, R. Selvaraj, Synthesis, biological and environmental applications of hydroxyapatite and its composites with organic and inorganic coatings, Prog. Org. Coatings. 151 (2021) 106056. https://doi.org/10.1016/j.porgcoat.2020.106056.
23. G. Bansal, R.K. Gautam, J.P. Misra, A. Mishra, Physiomechanical, Flowability, and Antibacterial Characterization of Silver-Doped Eggshell-Derived Hydroxyapatite for Biomedical Applications, J. Mater. Eng. Perform. (2023). https://doi.org/10.1007/s11665-023-08696-6.
24. A.J. Ansari, G. Bansal, S.A.H. Rizvi, Effect of reinforcement particles and multipass of friction stir processing on microstructure and mechanical properties of aluminium alloy, Mater. Lett. 355 (2024) 135555. https://doi.org/10.1016/j.matlet.2023.135555.
25. D.B. Singh, N. Kumar, A. Raturi, G. Bansal, A. Nirala, N. Sengar, Effect of Flow of Fluid Mass Per Unit Time on Life Cycle Conversion Efficiency of Double Slope Solar Desalination Unit Coupled with N Identical Evacuated Tubular Collectors, in: 2021. https://doi.org/10.1007/978-981-15-8542-5_34.
26. A. Maidaniuc, F. Miculescu, S.I. Voicu, C. Andronescu, M. Miculescu, E. Matei, A.C. Mocanu, I. Pencea, I. Csaki, T. Machedon-Pisu, L.T. Ciocan, Induced wettability and surface-volume correlation of composition for bovine bone derived hydroxyapatite particles, Appl. Surf. Sci. 438 (2018) 158–166. https://doi.org/10.1016/j.apsusc.2017.07.074.
27. M. Mirzaee, M. Vaezi, Y. Palizdar, Synthesis and characterization of silver doped hydroxyapatite nanocomposite coatings and evaluation of their antibacterial and corrosion resistance properties in simulated body fluid, Mater. Sci. Eng. C. 69 (2016) 675–684. https://doi.org/10.1016/j.msec.2016.07.057.
28. Q. Zhou, T. Wang, C. Wang, Z. Wang, Y. Yang, P. Li, R. Cai, M. Sun, H. Yuan, L. Nie, Synthesis and characterization of silver nanoparticles-doped hydroxyapatite/alginate microparticles with promising cytocompatibility and antibacterial properties, Colloids Surfaces A Physicochem. Eng. Asp. 585 (2020) 124081. https://doi.org/10.1016/j.colsurfa.2019.124081.
29. Q. Yuan, A. Xu, Z. Zhang, Z. Chen, L. Wan, X. Shi, S. Lin, Z. Yuan, L. Deng, Bioactive silver doped hydroxyapatite composite coatings on metal substrates: Synthesis and characterization, Mater. Chem. Phys. 218 (2018) 130–139. https://doi.org/10.1016/j.matchemphys.2018.07.038.
30. X. Shi, J. Zhou, G. Liu, L. Wang, The Physical and Antimicrobial Properties of Silver Doped Hydroxyapatite Sintered by Microwave and Conventional Sintering, J. Inorg. Organomet. Polym. Mater. 27 (2017) 955–961. https://doi.org/10.1007/s10904-017-0542-8.
31. M. Roy, G.A. Fielding, H. Beyenal, A. Bandyopadhyay, S. Bose, Mechanical, in vitro antimicrobial, and biological properties of plasma-sprayed silver-doped hydroxyapatite coating, ACS Appl. Mater. Interfaces. 4 (2012) 1341–1349. https://doi.org/10.1021/am201610q.

32. C.K. Patil, H.D. Jirimali, J.S. Paradeshi, B.L. Chaudhari, V. V. Gite, Functional antimicrobial and anticorrosive polyurethane composite coatings from algae oil and silver doped egg shell hydroxyapatite for sustainable development, Prog. Org. Coatings. 128 (2019) 127–136. https://doi.org/10.1016/j.porgcoat.2018.11.002.
33. P. Vijayaraghavan, M.A. Rathi, K.S. Almaary, F.S. Alkhattaf, Y.B. Elbadawi, S.W. Chang, B. Ravindran, Preparation and antibacterial application of hydroxyapatite doped Silver nanoparticles derived from chicken bone, J. King Saud Univ. - Sci. 34 (2022) 101749. https://doi.org/10.1016/j.jksus.2021.101749.
34. F. Nurfiana, A. Kadarwati, S. Putra, Synthesis and characterization of hydroxyapatite from duck eggshell modified silver by gamma radiolysis method, J. Phys. Conf. Ser. 1436 (2020) 012099. https://doi.org/10.1088/1742-6596/1436/1/012099.
35. D.K. Owens, R.C. Wendt, Estimation of the surface free energy of polymers, J. Appl. Polym. Sci. 13 (1969) 1741–1747. https://doi.org/10.1002/app.1969.070130815.
36. S. Sebastiammal, A.S. Lesly Fathima, S. Alarifi, S. Mahboob, J. Henry, M.R. Kavipriya, M. Govindarajan, M. Nicoletti, B. Vaseeharan, Synthesis and physicochemical characteristics of Ag-doped hydroxyapatite nanoparticles, and their potential biomedical applications, Environ. Res. 210 (2022) 112979. https://doi.org/10.1016/j.envres.2022.112979.
37. V. Ganesan, M. Devaraj, S.K. Govindan, V.S. Kattimani, G. Easwaradas Kreedapathy, Eggshell derived mesoporous biphasic calcium phosphate for biomedical applications using rapid thermal processing, Int. J. Appl. Ceram. Technol. 16 (2019) 1932–1943. https://doi.org/10.1111/IJAC.13270.
38. K.C.C. Vinoth Kumar, T. Jani Subha, K.G.G. Ahila, B. Ravindran, S.W.W. Chang, A.H. Mahmoud, O.B. Mohammed, M.A.A. Rathi, Spectral characterization of hydroxyapatite extracted from Black Sumatra and Fighting cock bone samples: A comparative analysis, Saudi J. Biol. Sci. 28 (2021) 840–846. https://doi.org/10.1016/j.sjbs.2020.11.020.
39. C. Chappard, G. André, M. Daudon, D. Bazin, Analysis of hydroxyapatite crystallites in subchondral bone by Fourier transform infrared spectroscopy and powder neutron diffraction methods, Comptes Rendus Chim. 19 (2016) 1625–1630. https://doi.org/10.1016/j.crci.2015.03.015.
40. S.L. Iconaru, P. Chapon, P. Le Coustumer, D. Predoi, Antimicrobial Activity of Thin Solid Films of Silver Doped Hydroxyapatite Prepared by Sol-Gel Method, Sci. World J. 2014 (2014) 1–8. https://doi.org/10.1155/2014/165351.
41. J.M. dos Santos Nunes Reis, C.E. Vergani, A.C. Pavarina, E.T. Giampaolo, A.L. Machado, Effect of relining, water storage and cyclic loading on the flexural strength of a denture base acrylic resin, J. Dent. 34 (2006) 420–426. https://doi.org/10.1016/j.jdent.2005.10.001.
42. W.L. Tham, W.S. Chow, Z.A.M. Ishak, Simulated body fluid and water absorption effects on poly(methyl methacrylate)/hydroxyapatite denture base composites, Express Polym. Lett. 4 (2010) 517–528. https://doi.org/10.3144/expresspolymlett.2010.66.
43. S. Eraković, A. Janković, D. Veljović, E. Palcevskis, M. Mitrić, T. Stevanović, D. Janaćković, V. Miskovic-Stankovic, Corrosion stability and bioactivity in simulated body fluid of silver/hydroxyapatite and silver/hydroxyapatite/lignin coatings on titanium obtained by electrophoretic deposition, J. Phys. Chem. B. 117 (2013) 1633–1643. https://doi.org/10.1021/jp305252a.
44. M. Nakamura, N. Hori, H. Ando, S. Namba, T. Toyama, N. Nishimiya, K. Yamashita, Surface free energy predominates in cell adhesion to hydroxyapatite through wettability, Mater. Sci. Eng. C. 62 (2016) 283–292. https://doi.org/10.1016/j.msec.2016.01.037.
45. S. V. Harb, N.J. Bassous, T.A.C. de Souza, A. Trentin, S.H. Pulcinelli, C. V. Santilli, T.J. Webster, A.O. Lobo, P. Hammer, Hydroxyapatite and β-TCP modified PMMA-TiO2 and PMMA-ZrO2 coatings for bioactive corrosion protection of Ti6Al4V implants, Mater. Sci. Eng. C. 116 (2020) 111149. https://doi.org/10.1016/J.MSEC.2020.111149.
46. A. Szcześ, Y. Yan, E. Chibowski, L. Hołysz, M. Banach, Properties of natural and synthetic hydroxyapatite and their surface free energy determined by the thin-layer wicking method, Appl. Surf. Sci. 434 (2018) 1232–1238. https://doi.org/10.1016/j.apsusc.2017.11.250.

47. M.R. Senra, R.B. de Lima, D. de H.S. Souza, M. de F.V. Marques, S.N. Monteiro, Thermal characterization of hydroxyapatite or carbonated hydroxyapatite hybrid composites with distinguished collagens for bone graft, J. Mater. Res. Technol. 9 (2020) 7190–7200. https://doi.org/10.1016/j.jmrt.2020.04.089.
48. S. Lazić, S. Zec, N. Miljević, S. Milonjić, The effect of temperature on the properties of hydroxyapatite precipitated from calcium hydroxide and phosphoric acid, Thermochim. Acta. 374 (2001) 13–22. https://doi.org/10.1016/S0040-6031(01)00453-1.
49. A. Tuna, Y. Okumuş, H. Çelebi, A.T. Seyhan, Thermochemical conversion of poultry chicken feather fibers of different colors into microporous fibers, J. Anal. Appl. Pyrolysis. 115 (2015) 112–124. https://doi.org/10.1016/j.jaap.2015.07.008.

